The X-ray Structure Factor of Liquid Glycerol

M. Soltwisch

Institut für Atom- u. Festkörperphysik, Freie Universität Berlin

and B. Steffen

Teilinstitut für Strukturforschung am Fritz-Haber-Institut der Max-Planck-Gesellschaft, Berlin

Z. Naturforsch. **36a**, 1045–1051 (1981); received December 24, 1980

The X-ray scattering intensity from highly viscous, liquid glycerol has been measured using MoK_α-radiation ($0.2 < q\,Å < 10$) between 250 K and 350 K. The corrected spectra were Fourier transformed to obtain the atomic radial distribution function.

For increasing temperatures one observes an increase of the X-ray intensity before the first structure maximum, and a broadening and a shift to lower-q-values of the main peak, while the peak height remains nearly constant.

The temperature dependent structure factors are compared with a model calculation, which in a simple way gives the correct compressibility limit. From the fits to the structure maximum the existence of orientational correlations is inferred.

1. Introduction

The spatial arrangement of nonspherical molecules forming a liquid is often described by interdependent center of mass and orientation correlations functions. The latter will depend on the structure of the molecule and on the interaction potential. Both correlation functions are, due to the thermal motion of the molecules, time dependent and experiments with high energy resolution like NMR, light-, neutron- and Mössbauer-scattering are suited to measure aspects of the time evolution of the correlation functions. For liquid glycerol $C_3O_3H_8$ several measurements of this kind exist (see [1, 2, 3, 5] and references cited therein). This liquid is highly associated, supercools easily, and the range of values which the diffusion coefficient assumes [4] extends continuously from $D \approx 10^{-13}$ cm^2/sec (at the glass transition temperature ~ 180 K) to values characteristic for normal liquids (> 400 K). If one tries to derive a translational energy E_{tr} from the translational diffusion, even a very rough estimate shows that $E_{tr} \ll k_B T$ below say 350 K. For details see e.g. the quasielastic neutron and Mössbauer scattering results [2, 3]. On the other hand the quasielastic part of the scattered intensity decreases with increasing T, similar to the Debye Waller factor [2, 3]. These facts suggest an attempt to treat scattering from glycerol in its liquid phase like scattering from an amorphous solid with phononlike vibrations.

To our knowledge so far no X-ray structure investigations of liquid glycerol were reported despite the fact that many dynamical studies are available. We have therefore measured the X-ray scattering for momentum transfer $q = 0.2$ to 10 Å^{-1}. The analysis of the data will not only have to deal with the temperature dependence of the molecular structure, but also with the effect of (acoustic) phonons on the intensities, with the possibility of a conformational change of the molecules when one goes from the crystalline to the liquid state, and with the effect of orientational correlations on the structure factor.

After describing the experiment in Sect. 2 and the theoretical background in Sect. 3, we compare in Sect. 4 the results with a simple model-structure-function which takes into account the effects just mentioned.

2. Experiment and Scattering Intensities

2.1. Experimental Set-up

The experiments were performed on an X-ray θ–θ-goniometer which has been described elsewhere [6]. The scattering chamber consists of brass with two parallel beryllium windows (diameter 30 mm) 2 mm apart. It was filled with dry glycerol and operated in Laue transmission geometry.

Reprint requests to Herrn Dr. M. Soltwisch, FB 20, WE 1A, Freie Universität Berlin, Boltzmannstraße 20, 1000 Berlin 33.

0340-4811 / 81 / 1000-1045 $ 01.00/0. — Please order a reprint rather than making your own copy.

Heating and cooling of the sample as well as the protection against humidity was the same as in a former Mössbauer experiment [2].

Measurements were performed using MoK_α radiation ($\lambda = 0.711$ Å) between $\theta = 0.6°$ and 35° in steps of 0.05°. The sample temperatures were $T = 250$ K, 275 K, 300 K, 325 K, 350 K.

2.2. Corrections and Normalization

The measured intensity distributions were corrected for empty container scattering, absorption and polarization. The correction for Compton-scattering was performed as follows: the necessary wavelength profile of the Compton inelastic scattering was calculated for several angles [7] and multiplied by a rectangular step function of width $\Delta\lambda$, given by the wavelenth acceptance curve of the monochromator. The resultant profile was then integrated over the wavelength and this value gave the Compton scattering intensity accepted by the monochromator at this scattering angle. In order to obtain the scattered intensity per molecule (in electron units (eu)), the Compton intensity of all atoms of the glycerol molecule was added up

$$I^{\mathrm{comp}}(\theta) = \sum_{\nu} \int_{\lambda_0}^{\lambda_0+\Delta\lambda} I_\nu^{\mathrm{comp}}(\theta, \lambda)\, \mathrm{d}\lambda\,. \qquad (1)$$

The X-ray atomic scattering factors $f_\nu(q)$ were taken from Cromer and Weber [8] with the dispersion corrections from Dauben and Templeton [9].

2.3. Experimental Results

Figure 1a shows the normalized intensity distributions $I_{\mathrm{ex}}(q)$ for $T = 250$ K and 350 K divided by the incoherent molecular scattering intensity $A_{\mathrm{in}} = \sum_\nu f_\nu^2(q)$ ($= 308$ eu at $q = 0$). With increasing temperatures one observes an increase of the intensity on the left hand side of the structure maximum, a shift of the latter to lower q-values, and a broadening of the peak itself. An increase at very low q (down to 0.2 Å^{-1}) is also observed. At this point the hydrodynamic region might be attained where an increase in intensity is partly due to an increase of the isothermal compressibility χ_T according to

$$I(q=0) = \varrho_{\mathrm{n}} k_{\mathrm{B}} T \chi_T \left(\sum_\nu f_\nu(0)\right)^2, \qquad (2)$$

where ϱ_{n} is the molecular number density. The low q-range is presented separately in Figure 4.

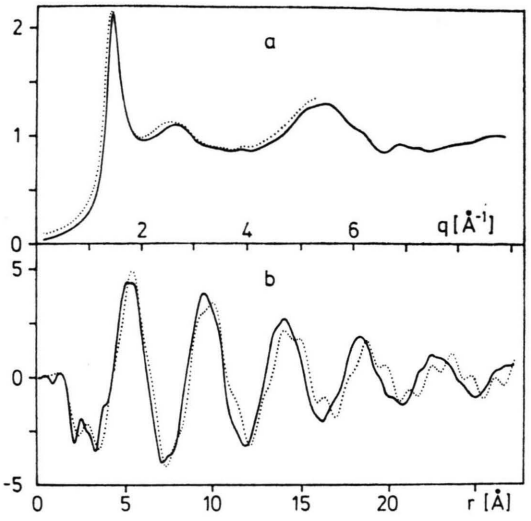

Fig. 1a. Experimental intensity distribution at $T = 250$ K (solid line) and at 350 K (dotted line) as function of momentum transfer $q = 4\pi \sin(\theta)/\lambda$. The spectra are corrected as explained in the text. Plotted is the ratio $I_{\mathrm{ex}}(q)/\sum_\nu f_\nu^2(q)$ where the denominator is the incoherent molecular form-factor. — 1b. One dimensional Fourier transform of $I_{\mathrm{ex}}(q) - \sum_\nu f_\nu^2(q)$, giving $4\pi r^2(\varrho(r) - \varrho_0)$, the radial distribution function with $\varrho(r)$ the density at r due to an average atom at $r = 0$, and ϱ_0 the mean density. The ordinate is in 10^2 eu/Å.

In Fig. 1b the one dimensional Fourier transform of the curve $\left| I_{\mathrm{ex}}(q) - \sum_\nu f_\nu^2(q) \right|$ is displayed, which is $4\pi r^2(\varrho(r) - \varrho_0)$, ϱ_0 being the electron density averaged over the sample.

These functions represent the average electronic density at distance r from the center of mass of a mean atom, where the electronic density distribution of this mean atom appears as an additional broadening of the peaks of the spatial distribution functions.

The fact that the 350 K curve in Fig. 1b shows more oscillations than the 250 K curve is due to the shorter q-range measured.

3. The Scattering Law

We shall assume that the liquid consists of one type of rigid molecules only (one conformation), and we separate the scattering intensity into self and distinct parts, $I(q) = I_{\mathrm{s}}(q) + I_{\mathrm{d}}(q)$. The center of mass (CM) of molecule i is $\boldsymbol{R}_i$. The atoms have positions $\boldsymbol{r}_\nu$ with respect to a molecular frame of reference, which itself has orientation $w_1 = (\theta_1, \varphi_1, \psi_1)$ with respect to the laboratory frame of

reference. Then the molecular scattering amplitude of molecule 1 is

$$A(\boldsymbol{q}, w_1) = \sum_{\nu} f_\nu(q) \exp[i\,\boldsymbol{q}(\boldsymbol{R}_1 + D(w_1)\,\boldsymbol{r}_\nu)], \quad (3)$$

where $D(w_1)$ is the rotation matrix connecting the reference frames.

The self part of $I(q)$ is

$$I_s(q) = \langle A^2(\boldsymbol{q}, w)\rangle = \sum_{\nu\mu} f_\nu f_\mu \sin(q r_{\nu\mu})/q r_{\nu\mu} = \langle A(\boldsymbol{q}, w)\rangle^2 + \sum_{l=1}^{\infty} \sum_{\nu\mu} f_\nu f_\mu (2l+1) \cdot j_l(q r_\nu)\, j_l(q r_\mu)\, P_l(\cos\theta_{\nu\mu}). \quad (4)$$

The averaging over orientation w is denoted by brackets. $\theta_{\mu\nu}$ is the angle between $\boldsymbol{r}_\mu$ and $\boldsymbol{r}_\nu$ within one molecule, $r_{\mu\nu} = |\boldsymbol{r}_\mu - \boldsymbol{r}_\nu|$, $j_l(qr)$ are the spherical Bessel functions, and $P_l(\cos\theta_{\nu\mu})$ the Legendre polynominals.

The distinct part becomes

$$I_d(q) = \int A(\boldsymbol{q}, w_1)\, A(\boldsymbol{q}, w_2) \cdot F_d(\boldsymbol{q}, w_1, w_2)\, dw_1\, dw_2, \quad (5)$$

where $F_d(\boldsymbol{q}, w_1, w_2)$ is the Fourier transform of the distinct correlation function which gives the probability to find a molecule at $\boldsymbol{R}_2$ with orientation w_2, given that there is a molecule at $\boldsymbol{R}_1$ with orientation w_1.

If there is no orientational correlation, the integration in (5) can be performed, $F_d(\boldsymbol{q}, w_1, w_2)$ becomes simply the CM-correlation function $F_d(q)$, and

$$I(q) = \langle A^2(q)\rangle + \langle A(q)\rangle^2 F_d(q). \quad (6)$$

One may look at (6) as the first term in an expansion

$$F_d(\boldsymbol{q}, w_1, w_2) = F_d(q) + F_{OR}(\boldsymbol{q}, w_1, w_2).$$

Restricting ourselves to the term (6), we have to discuss the molecular structure, A, and the CM-CF, $F_d(q)$. The effect of the next term, the orientational correlation function (OR-CF), $F_{OR}(\boldsymbol{q}, w_1, w_2)$, will be considered in Section 4. While the present simple treatment derives from [2], more elaborate formulations have been presented e.g. by Zeidler et al. [10].

3.1. *Molecular Structure*

A first guess for $A(\boldsymbol{q}, w)$ is the molecular structure in crystalline glycerol as measured by Koningsveld [11] using X-rays. The carbon and oxygen positions which he found are given in Table 1. This

Table 1. Atomic coordinates [Å] in the glycerol molecule in crystalline phase [11] (carbons and oxygens only). The $O_3^{+)}$ coordinates were created by a 180°-rotation of O_3 around the C_2-C_3-axis (compact shape).

	x	y	z
O_1	0.87	6.95	0.50
O_2	1.70	5.40	2.74
O_3	− 0.33	4.10	4.20
$O_3^{+)}$	− 1.34	6.37	3.86
C_1	0.14	6.90	1.74
C_2	0.34	5.50	2.33
C_3	− 0.54	5.30	3.60

is the so called αα-conformation with no intramolecular hydrogen bonds possible. The shape of the molecule is rather elongated and the association occurs via intermolecular hydrogen bonds.

In order to study the influence of the molecular structure in the liquid, we have calculated A for several conformations. Looking at the isolated molecule, a conformational change to a more compact form can easily be performed by rotating an oxygen O3 (and/or O1) around the C2-C3 (and/or C2-C1) axis, leading to intramolecular bonding. The results for $\langle A^2\rangle$ and $\langle A\rangle^2$ are presented in Figure 2. Normalized to the sum of the atomic scattering intensities $\sum f_\nu^2$, we show the molecular intensity averaged over orientation, $\langle A^2\rangle$, as well as the intensity due to the nonspherical shape of the molecule $\langle A^2\rangle - \langle A\rangle^2$. The latter is equivalent to the sum of all nonzero moments if one expands the

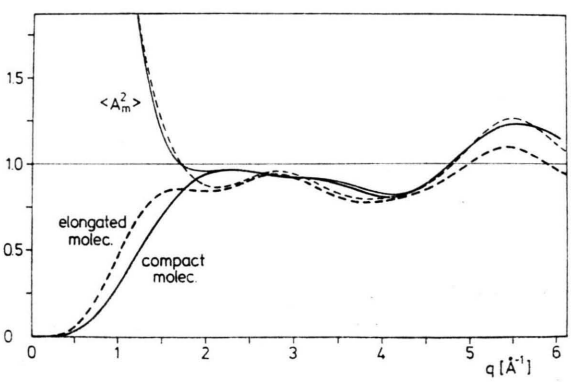

Fig. 2. $(\langle A^2\rangle - \langle A\rangle^2)/\sum_\nu f_\nu^2(q)$, deviation of the molecular formfactors $\langle A^2\rangle$ from the mean values $\langle A\rangle^2$ for two conformations (thick lines). Thin lines correspond to $\langle A^2\rangle$. Dashed lines: elongated molecular shape from crystalline structure. Solid lines: compact shape by rotating O_3 about 180° around C_2-C_3-axis (see Table 1, [11]). $A_m^2 = A^2/\sum_\nu f_\nu^2$.

scattered intensity into spherical harmonics [1], see (4). The effect of a change of the molecular shape on the total structure function is rather drastic around $q = 1$ Å^{-1} as can be concluded from Figure 2. However, the steep rise of $F_d(q)$ falls in the same region, and the OR-CF is also important there.

3.2. Center of Mass Correlation and Thermal Diffuse Scattering

For low q, homogeneous systems are rather transparent ($F_d(q) \approx -1$) except for the long wavelength density fluctuations due to thermally excited phonons which are responsible for the compressibility limit, cf. (2). This limit is easy to verify if one uses the scattering law for a crystalline powder and evaluates it within the zeroth Brillouin zone (BZ). To the extent that longitudinal sound waves are the main contributors to $I(q \to 0)$, this calculation should also be valid for the center of mass scattering of glycerol $F_d(q)$ up to q about half the structure maximum position.

One gets (up to two phonon processes)

$$F_d(q) + 1 = S(q) = \frac{e^{-2M}}{\alpha}\left[\delta(\boldsymbol{q}) + \alpha \frac{k_B T}{m v^2} q^2 \int_{BZ} \frac{\delta(\boldsymbol{q}+\boldsymbol{g}_1)}{g_1^2}\,\mathrm{d}^3 g_1 + \alpha^2 \left(\frac{k_B T}{m v^2}\right)^2 \frac{q^4}{2} \int_{BZ} \delta(\boldsymbol{q}+\boldsymbol{g}_1+\boldsymbol{g}_2)\,\mathrm{d}^3 g_1\,\mathrm{d}^3 g_2\right] + \cdots$$
$$\approx e^{-2M}\left[\delta(\boldsymbol{q})/\alpha + \frac{k_B T}{m v^2}\left(1 + \frac{k_B T}{m v^2}\frac{V_z}{16} q^3\right)\right] \tag{7}$$

with v = velocity of sound; V_z = volume of primitive cell; $\boldsymbol{g}$ = phonon wave vector; m = molecular mass; $\alpha = V_z/(2\pi)^3$. For an extensive discussion and the higher terms, see e.g. [12]. We shall omit the forward scattering due to $\delta(\boldsymbol{q})$. The Debye Waller exponent is small in the first BZ: $2M = q^2\langle x^2\rangle = 3 k_B T/m v^2 \cdot q^2/q_D^2 \approx 0$ ($q/q_D \ll 1$; q_D = Debye-radius of BZ; $\langle x^2\rangle$ = mean squared vibrational amplitude). One then has to a good approximation for $q \to 0$

$$S(q) = \frac{k_B T}{m v^2}\left[1 + \frac{k_B T}{m v^2}\frac{3\pi^2}{8}\frac{q^3}{q_D^3}\right]. \tag{8}$$

From

$$\frac{c_v}{c_p}\varrho_n \chi_T = \frac{N}{V^2}\frac{\partial V}{\partial p} = \frac{N}{V^2}\frac{E}{p^2} = \frac{1}{m v^2} \tag{9}$$

with $p = E/V$ the pressure; $E = N m v^2$ the mean internal energy; $c_p \approx c_v$ the specific heats, one recovers from (8) the result for the limit $q = 0$,

$$S(q=0) = \varrho_n \chi_T k_B T. \tag{10}$$

This form leads back to (2).

From (7) it is obvious that in the absence of small angle scattering due to clustering the low q region of the scattering law produces purely inelastic scattering (Brillouin scattering). The q independence of the one phonon scattering stems from the high temperature limit adopted throughout. A more accurate evaluation produces a weak increase of this part with q.

Because we were interested in the evaluation of the ratio of elastic to inelastic scattering also at higher q (there the acoustic modes should strongly be disturbed by the loss of long range order and uncorrelated vibrations will dominate) we have extended the crystalline approach to this q-range. The existence of short range order, but loss of long range order was simulated by considering an fcc-lattice with a distribution $f(x)$ of lattice constants x around the mean value a

$$f(x) = \frac{x^2}{\sqrt{\pi}(a^2 \Delta + \frac{1}{2}\Delta^3)} \exp\left\{-\left(\frac{a-x}{\Delta}\right)^2\right\}. \tag{11}$$

This gaussian has two adjustable parameters, the mean lattice constant a and a smearing parameter Δ. Both were fitted to the experimental spectra to meet the first structure maximum in position and width. In doing so, the parameters fixing the phonon contributions were kept constant, and these contributions were calculated up to four phonon processes; it turned out that this is necessary to meet the total X-ray intensity, especially in the high q-range.

3.3. The Total Structure Function, Elastic and Inelastic Contribution

From the model and assumptions described, the following expression for $I(q)$ was derived for

comparison with the experimental results:

$$I(q) = S(q)[\langle A\rangle^2 + A_{OR}] + S_s(q)\{\langle A^2\rangle - [\langle A\rangle^2 + A_{OR}]\} \quad (12)$$

with

$$A_{OR} = \int A(\boldsymbol{q}, w_1)\, A(\boldsymbol{q}, w_2) \cdot F_{OR}(\boldsymbol{q}, w_1, w_2)\, dw_1\, dw_2 / F_d(q),$$

$$S(q) = S_0(q) + \sum_{m=1}^{\infty} S_m(q) = S_{el.} + S_{inel.}$$

and

$$S_s(q) = e^{-q^2\langle x^2\rangle} + (1 - e^{-q^2\langle x^2\rangle}) = S_{s.el.} + S_{s.inel.}$$

the self term of the center of mass scattering law.

The terms $S_m(q)$, $m = 0, 1, \ldots$ accounts for the phonon contributions (zero phonon, one phonon etc.). The OR-CF was set to zero for the fits.

4. Comparison with Experiment and Discussion

The result of the comparison of our simple model-function (12) with the measured structure factor is given in Fig. 3 for $T = 250$ K and in Fig. 4 for the low q-range for all temperatures. The input data

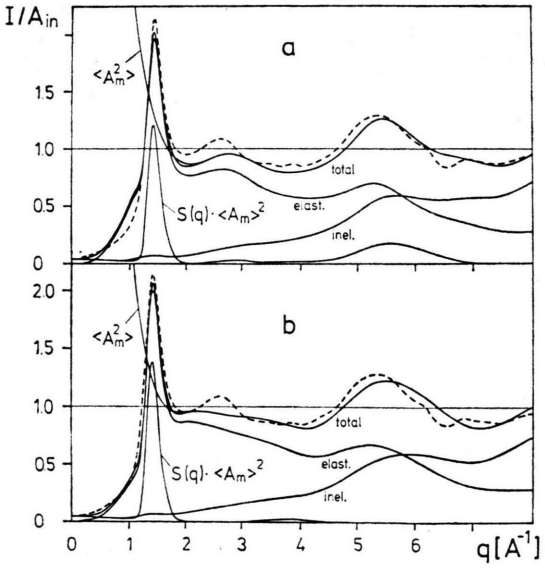

Fig. 3. Scattering as calculated from the model (solid lines) and experimental results (dashed lines) for $T = 250$ K. The total intensity is the sum of the elastic (zero phonon) and inelastic (up to 4th order phonons) intensities. The parameters used are $a = 7.15$ Å, $\Delta = 0.75$ Å, $v = 2110$ m/s. Fig. 3a: elongated molecule, Fig. 3b: compact molecule. $A_m^2 = A^2/\sum_p f_p^2 = A^2/A_{in}$.

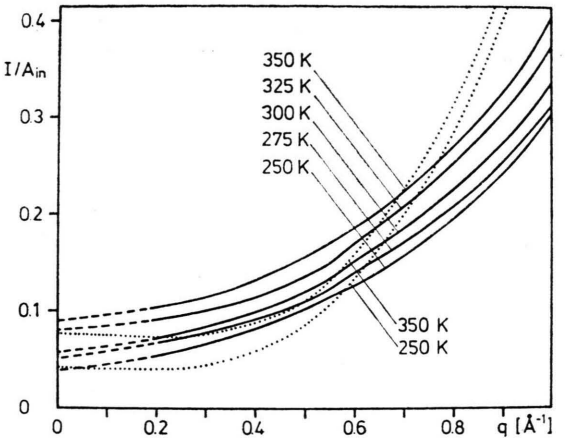

Fig. 4. Low q-range plot of all experimental curves (solid lines) and two theoretical curves (dotted lines, elongated molecule). The dashed lines are an eye-extrapolation to $q = 0$. The uncorrelated oscillations of the experimental curves are due to the statistical uncertainties.

for the inelastic contribution to $S(q)$ are collected in Table 2. We used the velocity of sound computed from the isothermal compressibility [13]. The parameters a, Δ were obtained by selecting by eye the curves $I(q)$ which fitted best the structure maximum. They are $a = 7.15$ Å ± 0.02, $\Delta = 0.75$ Å ± 0.05; the errors quoted are rough estimates, essentially independent of the molecular configuration. The next neighbour distance is $d = a/\sqrt{2}$.

In the low q-range ($q < 0.5$ Å) the inelastic intensity is dominant. The extrapolated values of the measured intensities at $q = 0$ meet the compressibility values within 20%, see Figure 4. This result would not be achieved in the case of uncorrelated vibrations (Einstein oscillators) since finite energy modes produce zero intensity at $q = 0$.

At the structure maximum one gets also a small inelastic peak. Such a peak is very pronounced in crystals, but due to the distribution of lattice constants which we use, the phonon structure is also

Table 2. Input data for calculation of inelastic scattering. Compressibility χ_T [13] and sound velocity v_χ derived from it. v_0 [14] is from ultrasonic measurement (low frequency part).

T[K]	χ_T[10^{-6} atm^{-1}]	v_χ[m/s]	v_0[m/s]
250	17.0	2110	2010
275	19.0	2035	1950
300	21.0	1960	1890
325	23.0	1876	1830
350	25.0	1830	1780

broadened. At still higher q the inelastic scattering derived from correlated or uncorrelated vibrations differs very little. The mean squared vibrational amplitude $\langle x^2 \rangle$ was 0.02 Å^2 at 250 K and 0.04 Å^2 at 350 K, which is much lower than derived from quasielastic scattering [2].

The distance between next neighbour molecules increases from 5.06 Å at 250 K to 5.16 Å at 350 K, an increase of $(2 \pm 0.5)\%$ in good agreement with the 1.6% from thermal expansion data [13].

The distribution parameter Δ is about $(10 \pm 2)\%$ of the next neighbour distance for all temperatures.

From the overall fit to the experimental curves two main features should be discussed:

If one uses for the molecular form factor the crystalline, elongated conformation, Fig. 3a, the computed total intensity is too high for $0.5 < q$ Å < 1 and too low for $1.8 < q$ Å < 2.8, the region of the second experimental structure peak. In Fig. 3b the compact conformation of the molecule was assumed. The discrepancy on the left side of the main peak is removed but the indication of a second peak near 2.7 Å^{-1} has disappeared.

The differences at the higher q-range $q > 3$ Å^{-1} between both conformations are not considered significant. The deviation of the third peak position may arise from an error in the average intramolecular distances. Due to the limited q-range actually measured, the normal access to the molecular formfactors by fitting only the high q-range [15] is for the present case of no value.

We turn now to orientational correlations and their interplay with possible molecular shapes. In Fig. 3 the term $S(q) \cdot \langle A \rangle^2$, is — according to our assumptions so far — the only term sensitive to nearest neighbours. (It is constructively interfering scattering from the average spherical electron density, i.e. the $l = 0$ term in (4), of neighbour molecules.) This term drops sharply for both conformations at $q > 1.9$ Å^{-1}, because $\langle A \rangle^2$ becomes very small (see (4) and Figure 2). This has the consequence that the second peak of $S(q)$, which occurs at $q = 2.9$ Å^{-1}, does not show up in $S(q) \cdot \langle A \rangle^2$.

If one now involves orientational correlations also, the following interpretation of the experiment seems to be possible:

Except for the zeroth moment all higher scattering moments, $\langle A^2 \rangle - \langle A \rangle^2$, produce an appreciable intensity for q-values > 1 Å^{-1}, see Figure 2. If the A_{OR} are different from zero this has relatively little effect on the first term of (12) for $0.5 < q$ Å < 1, because there $\langle A \rangle^2 \gg A_{OR}$. On the other hand, the second term would be remarkably reduced by A_{OR} because $\langle A^2 \rangle - \langle A \rangle^2$ is small, perhaps comparable to A_{OR}. The necessary depression of the calculated curve in Fig. 3a at $q \approx 1$ Å can thus be achieved either by the compact shape (as discussed above) or by including orientational correlation. On the right hand side of the main peak our model function is so far fully determined by single molecular scattering ($S(q) \cdot \langle A \rangle^2 \approx 0$). It appears not unreasonable to expect that $A_{OR} F_d$ has an oscillating shape similar to F_d. Such a peak, if situated at $q = 2.6$ Å^{-1}, would offer an explanation for the experimental peak at this q: The higher scattering moments are practically constant beyond 2 Å^{-1}, see Fig. 2, and the intensity will thus reproduce the q-dependence of A_{OR} through the first term of (12).

The deviations of the model function, Fig. 3a, from the experimental structure factor on both sides of the main structure peak can thus be corrected by including orientational correlations, whereas starting with Fig. 3b, one would trade an improvement at $q = 2.6$ Å for a worsening of the agreement at 1 Å^{-1}. We thus conclude that the elongated molecular shape and non negligible orientational correlations are the more plausible situation.

5. Summary

We have presented a set of X-ray measurements on liquid glycerol and compared the data with a simple model for an amorphous structure which is including acoustic phonons. The intensity extrapolated to $q = 0$ is in good agreement with the isothermal sound velocity. The model allows a straightforward calculation of the elastic and inelastic scattered intensity (effective Debye-Waller factor) for the whole q-range.

The experimental scattering intensity displays a lot of details which we have tried to interprete using the model mentioned. From a consideration of the interrelated effects of molecular formfactors (average conformation of the molecule in the liquid), center of mass correlations, and orientational correlations it was concluded that the crystalline conformation of the molecule appears to be predomi-

nant in the liquid phase also and that orientational correlations seem to have a peak at $q \approx 2.6$ Å^{-1}.

The use of a crystalline lattice function with a distribution of lattice constants for the molecular center of mass correlation function is certainly a crude assumption for higher q-values, while it is reasonably correct in the hydrodynamic limit. It should be understood as a simple means for an estimate of the thermal diffuse scattering from amorphous structures to which strongly supercooling liquids may be assigned.

Acknowledgement

We would like to thank D. Quitmann for his kind interest in this work and his substantial help in performing the manuscript.

[1] M. Soltwisch, M. Elwenspoek, and D. Quitmann, Molec. Phys. **34**, 33 (1977).
[2] M. Elwenspoek, M. Soltwisch, and D. Quitmann, Molec. Phys. **35**, 1221 (1978).
[3] M. Soltwisch and D. Quitmann, J. Physique **40**, C2-666 (1979).
[4] D. J. Tomlinson, Molec. Phys. **25**, 735 (1972).
[5] H. Dux and Th. Dorfmüller, Chem. Phys. **40**, 219 (1979).
[6] B. Steffen, Phys. Rev. B **13**, 3227 (1975).
[7] J. Urban and D. Weick, J. Appl. Phys. **50**, 5947 (1979).
[8] D. T. Cromer and J. T. Weber, Acta Cryst. **18**, 104 (1965).
[9] C. H. Dauben and D. H. Templeton, Acta Cryst. **8**, 841 (1955).
[10] H. Bertagnolli, D. O. Leicht, and M. D. Zeidler, Molec. Phys. **36**, 1769 (1978).
[11] H. van Koningsveld, Recueil, **87**, 243 (1968).
[12] B. E. Warren, X-Ray Diffraction (Addison-Wesley) (1969).
[13] A. A. Newman, Glycerol (Morgan Grampian) (1968).
[14] R. Meister, C. J. Marhoeffer, R. Sciamanda, L. Cotter, and T. Litovitz, J. Appl. Phys. **31**, 854 (1960).
[15] L. Blum and A. H. Narten, Adv. in Chem. Phys. **34**, 203 (1976).